The role of attractive interactions in rod-sphere mixtures

ANTYPOV, D. and CLEAVER, D. J.

Published version

ANTYPOV, D. and CLEAVER, D. J. (2004). The role of attractive interactions in rod-sphere mixtures. Journal of chemical physics, 120 (21), 10307-10316.

The role of attractive interactions in rod-sphere mixtures

[1,2]Dmytro Antypov and [1]Douglas J. Cleaver

[1] Materials Research Institute, Sheffield Hallam University, Pond Street, Sheffield S1 1WB, United Kingdom.

[2] Max Planck Institute for Polymer Research, Ackermannweg 10, 55128 Mainz, Germany.

Abstract

We present a computer simulation study of binary mixtures of prolate Gay-Berne particles and Lennard-Jones spheres. Results are presented for three such rod-sphere systems which differ from each other only in the interaction between unlike particles. Both the mixing-demixing behavior and the transitions between the isotropic and any liquid crystalline phases are studied for each system, as a function of temperature and concentration ratio. For systems which show macroscopic demixing, the rod-sphere interaction is shown to give direct control over interfacial anchoring properties, giving rise to the possibility of micellar phase formation in the case of homeotropic anchoring. Additionally, it is shown that on incorporating high concentrations of spheres into a system of rods with weak demixing properties, microphase-separated structures can be induced, including bicontinuous and lamellar arrangements.

I INTRODUCTION

Virtually all practical applications of liquid crystals (LCs) employ multi-component materials. Whilst many of the components incorporated into these mixtures are liquid crystalline, others are included at low concentrations to yield specific mechanical behavior (e.g. chiral dopants in a twisted nematic display) or optical properties (e.g. dye molecules) whilst making no intrinsic mesogenic contribution.

At higher concentrations, non-mesogenic additives can both affect the structural and dynamic properties of the LC host and introduce extensive biphasic regions; their introduction also raises the possibility of novel phase formation. An early study of a molecular mesogen mixed with 10% by weight of non-mesogen found behavior characteristic of macrophase separation but suffered from persistent metastable states [1]. Subsequently, Loudet and co-workers developed oil in LC mixtures which, on quenching into the biphasic region, repeatably formed networks of highly monodisperse oil droplets in the LC solvent [2]. Through judicious introduction of surfactant species to tune the interfacial properties of these droplets, it has now proved possible to control the anchoring properties of, and, hence, the structures formed by, these LC colloid systems [3].

On a larger lengthscale, Vliegenthart and co-workers have found that low concentrations of colloidal needles act as very efficient depletion agents when added to spherical colloidal systems [4]. A more extensive experimental investigation of colloidal rod-sphere mixtures, which covered a broad range of relative concentrations, subsequently observed both macrophase separation and lamellar structures [5]. The latter, in which layers of spheres reside between layers of rods, are an example of a microphase separated arrangement. Prior to their observation in these colloidal systems, their existence had been predicted by Koda *et al* on purely entropic grounds [6] for mixtures of hard spheres and hard parallel spherocylinders. The characteristics underlying the stability of this lamellar arrangement were later investigated through a more wide-ranging study of such mixtures which employed a combination of second-virial theory and Monte Carlo simulation [7].

As well as this microphase-separated arrangement, entropy-driven macroscopic

demixing and macrophase separation have also been seen for model rod-sphere systems. Both mean-field theory and Monte Carlo simulation have been used to determine the phase behaviour of lattice-based models of binary LC-isotropic fluid mixtures [8]. Additionally, theoretical studies of hard rod-sphere mixtures in the orientationally isotropic phase have predicted circumstances (such as a significant difference between the sphere radius and the radius of the rod about its symmetry axis) in which demixing into coexisting rod-rich and sphere-rich phases is expected [9]. This was borne out by our previous study of mixtures of hard Gaussian overlap particles and hard spheres, for which these two radii were kept equal, since these remained well mixed in both isotropic and nematic phases for most volume fractions [10]. While this system did macrophase separate at high volume fractions, it showed no tendency to form lamellar or any other microphase separated arrangements; this is consistent with the predictions of Koda *et al's* theory for this particular combination of particle shapes [11].

In this paper, we investigate the effects that attractive interactions can induce in rod-sphere mixture systems. For this, we employ a generic model system comprising Lennard-Jones spheres and prolate Gay-Berne particles for which the single-component phase behavior is well characterized. This system can be considered as a model mixture of a molecular LC and a non-mesogenic molecular substance. Using our previous study of the equivalent hard-particle model [10] as a guide to the limiting behavior of these systems, we concentrate particularly on the influence of the rod-sphere interaction potential on the phases formed. Specifically, we show that a rich diversity of behavior can be obtained through modification of the strength and symmetry of this single interaction.

The structure of the remainder of this paper is as follows. In Sec. II we describe the model potentials used in our simulations. The simulation results are then presented in Sec. III with discussion and conclusions being given in Sec. IV.

II MODEL SYSTEMS

In this study, we assess the effect of the rod-sphere interaction on the phase behavior of rod-sphere mixtures. To do this, we employ models which are well characterized in the single component limit; for the sphere-sphere and rod-rod interactions, we use the Lennard-Jones and Gay-Berne potentials, respectively. The former is given by

$$U^{LJ}(r_{ij}) = 4\epsilon_0 \left(\left(\frac{\sigma_0}{r_{ij}} \right)^{12} - \left(\frac{\sigma_0}{r_{ij}} \right)^{6} \right), \tag{1}$$

where σ_0 and ϵ_0 are constants that set the length and energy scales and r_{ij} is the separation of particles i and j. The Gay-Berne interaction between a pair of rod-like molecules is given by [12]

$$U^{GB}(\mathbf{r_{ij}}, \hat{\mathbf{u}}_\mathbf{i}, \hat{\mathbf{u}}_\mathbf{j}) = 4\epsilon(\hat{\mathbf{r}}_\mathbf{ij}, \hat{\mathbf{u}}_\mathbf{i}, \hat{\mathbf{u}}_\mathbf{j}) \left[\left(\frac{\sigma_{GB}}{r_{ij} - \sigma(\hat{\mathbf{r}}_\mathbf{ij}, \hat{\mathbf{u}}_\mathbf{i}, \hat{\mathbf{u}}_\mathbf{j}) + \sigma_{GB}} \right)^{12} - \left(\frac{\sigma_{GB}}{r_{ij} - \sigma(\hat{\mathbf{r}}_\mathbf{ij}, \hat{\mathbf{u}}_\mathbf{i}, \hat{\mathbf{u}}_\mathbf{j}) + \sigma_{GB}} \right)^{6} \right], \tag{2}$$

where $\hat{\mathbf{r}}_\mathbf{ij} = \mathbf{r_{ij}}/r_{ij}$ is a unit vector along the intermolecular vector $\mathbf{r_{ij}} = \mathbf{r_i} - \mathbf{r_j}$ and the unit vectors $\hat{\mathbf{u}}_\mathbf{i}$ and $\hat{\mathbf{u}}_\mathbf{j}$ denote the rods' orientations. The shape anisotropy parameter, $\sigma(\hat{\mathbf{r}}_\mathbf{ij}, \hat{\mathbf{u}}_\mathbf{i}, \hat{\mathbf{u}}_\mathbf{j})$, and the well-depth anisotropy function, $\epsilon(\hat{\mathbf{r}}_\mathbf{ij}, \hat{\mathbf{u}}_\mathbf{i}, \hat{\mathbf{u}}_\mathbf{j})$, are given by

$$\sigma(\hat{\mathbf{r}}_\mathbf{ij}, \hat{\mathbf{u}}_\mathbf{i}, \hat{\mathbf{u}}_\mathbf{j}) = \sigma_{GB} \left[1 - \frac{\chi}{2} \left\{ \frac{(\hat{\mathbf{r}}_\mathbf{ij} \cdot \hat{\mathbf{u}}_\mathbf{i} + \hat{\mathbf{r}}_\mathbf{ij} \cdot \hat{\mathbf{u}}_\mathbf{j})^2}{1 + \chi(\hat{\mathbf{u}}_\mathbf{i} \cdot \hat{\mathbf{u}}_\mathbf{j})} + \frac{(\hat{\mathbf{r}}_\mathbf{ij} \cdot \hat{\mathbf{u}}_\mathbf{i} - \hat{\mathbf{r}}_\mathbf{ij} \cdot \hat{\mathbf{u}}_\mathbf{j})^2}{1 - \chi(\hat{\mathbf{u}}_\mathbf{i} \cdot \hat{\mathbf{u}}_\mathbf{j})} \right\} \right]^{-1/2} \tag{3}$$

and

$$\epsilon(\hat{\mathbf{r}}_\mathbf{ij}, \hat{\mathbf{u}}_\mathbf{i}, \hat{\mathbf{u}}_\mathbf{j}) = \epsilon_{GB} \left[\epsilon_1(\hat{\mathbf{u}}_\mathbf{i}, \hat{\mathbf{u}}_\mathbf{j}) \right]^\nu \left[\epsilon_2(\hat{\mathbf{r}}_\mathbf{ij}, \hat{\mathbf{u}}_\mathbf{i}, \hat{\mathbf{u}}_\mathbf{j}) \right]^\mu. \tag{4}$$

Here, μ and ν are adjustable parameters and $\epsilon_1(\hat{\mathbf{u}}_\mathbf{i}, \hat{\mathbf{u}}_\mathbf{j})$ and $\epsilon_2(\hat{\mathbf{r}}_\mathbf{ij}, \hat{\mathbf{u}}_\mathbf{i}, \hat{\mathbf{u}}_\mathbf{j})$ are given by

$$\epsilon_1(\hat{\mathbf{u}}_\mathbf{i}, \hat{\mathbf{u}}_\mathbf{j}) = \left[1 - \chi^2 (\hat{\mathbf{u}}_\mathbf{i} \cdot \hat{\mathbf{u}}_\mathbf{j})^2 \right]^{-1/2}, \tag{5}$$

and

$$\epsilon_2(\hat{\mathbf{r}}_\mathbf{ij}, \hat{\mathbf{u}}_\mathbf{i}, \hat{\mathbf{u}}_\mathbf{j}) = 1 - \frac{\chi'}{2} \left\{ \frac{(\hat{\mathbf{r}}_\mathbf{ij} \cdot \hat{\mathbf{u}}_\mathbf{i} + \hat{\mathbf{r}}_\mathbf{ij} \cdot \hat{\mathbf{u}}_\mathbf{j})^2}{1 + \chi'(\hat{\mathbf{u}}_\mathbf{i} \cdot \hat{\mathbf{u}}_\mathbf{j})} + \frac{(\hat{\mathbf{r}}_\mathbf{ij} \cdot \hat{\mathbf{u}}_\mathbf{i} - \hat{\mathbf{r}}_\mathbf{ij} \cdot \hat{\mathbf{u}}_\mathbf{j})^2}{1 - \chi'(\hat{\mathbf{u}}_\mathbf{i} \cdot \hat{\mathbf{u}}_\mathbf{j})} \right\}. \tag{6}$$

The parameters χ and χ' in Eqs.(3), (5) and (6) are associated with the shape and energy anisotropy of the Gay-Berne particles. χ is a function of the rod length to

breadth ratio l/d and is given by

$$\chi = \frac{(l/d)^2 - 1}{(l/d)^2 + 1}. \tag{7}$$

The parameter χ', meanwhile, is determined from the ratio of end-end to side-side well depths via

$$\chi' = \frac{1 - (\epsilon_{ee}/\epsilon_{ss})^{(1/\mu)}}{1 + (\epsilon_{ee}/\epsilon_{ss})^{(1/\mu)}}. \tag{8}$$

While the constants σ_0 and σ_{GB} in Eqs. (1) and (2) are, in principle, independent, we equate them in the work presented here. This means that the diameters of the spheres are equal to the breadths of the rods. Similarly, we set the well depths ϵ_0 and ϵ_{GB} equal to one another. Finally, the Gay-Berne model contains four adjustable parameters: the elongation l/d, the energy anisotropy $\epsilon_{ee}/\epsilon_{ss}$ and the exponents μ and ν. Here, we adopt the frequently used parameterization $l/d = 3$, $\epsilon_{ss}/\epsilon_{ee} = 5$, $\mu = 2$ and $\nu = 1$ for which the bulk phase behavior is well established [13].

For the rod-sphere potential, we adopt the appropriate limit of Eq.(3) originally noted by Berne and Pechukas [14]. Thus, for the case where particle j is a rod and particle i is a sphere with diameter equal to the rod's breadth, the shape parameter is expressed as

$$\sigma(\hat{\mathbf{r}}_{\mathbf{ij}}, \hat{\mathbf{u}}_{\mathbf{j}}) = \sigma_0 \left[1 - \chi(\hat{\mathbf{r}}_{\mathbf{ij}} \cdot \hat{\mathbf{u}}_{\mathbf{j}})^2\right]^{-1/2}. \tag{9}$$

The energy parameter we adopt for the rod-sphere interaction is [15]

$$\epsilon(\hat{\mathbf{r}}_{\mathbf{ij}}, \hat{\mathbf{u}}_{\mathbf{j}}) = \epsilon_{RS} \left[1 - \left(1 - \left(\frac{\epsilon_E}{\epsilon_S}\right)^{1/\mu}\right)(\hat{\mathbf{r}}_{\mathbf{ij}} \cdot \hat{\mathbf{u}}_{\mathbf{j}})^2\right]^{\mu}, \tag{10}$$

where ϵ_{RS} is a constant and the ratio ϵ_S/ϵ_E controls the configurational side-to-end well-depth anisotropy of the interaction. In this paper, we examine the effect of the rod-sphere interaction on phase behavior by varying the two parameters ϵ_{RS} and ϵ_S/ϵ_E in Eq. (10), while keeping the rod-sphere shape parameter (9) and all aspects of the rod-rod and sphere-sphere interactions unchanged.

In the first parameterization to be considered here (system (i)), we set $\epsilon_S/\epsilon_E = \epsilon_{ss}/\epsilon_{ee} = 5$ such that the spheres favor the sides of the rods rather than the ends. By changing the ratio ϵ_S/ϵ_E, however, it is possible to create systems in which spheres favor the ends of the rods rather than the sides ($\epsilon_S/\epsilon_E = 0.2$ - system (ii)) or in

which the spheres make no distinction between different parts of the rods ($\epsilon_S/\epsilon_E = 1$ - system (iii)). Equipotential lines of rod-sphere potentials representing these three cases are shown in Fig. 1. The parameter ϵ_{RS} can also be varied independently of the ratio of the rod-rod and rod-sphere well depths. This both defines the mixing rules and offers a useful normalization with which to balance the average rod-sphere interaction strength against those of the rod-rod and sphere-sphere interactions. We have made use of this in system (ii); setting ϵ_{RS}/ϵ_0 to 0.2 for this system ensures that its rod-sphere interaction strengths are broadly similar to those in system (i). For the sake of clarity, the rod-sphere parameterizations for the three systems considered in this paper are given in Tab. I, along with ϵ_S and ϵ_E, the well-depths experienced when the vectors $\hat{\mathbf{r}}_{\mathbf{ij}}$ and $\hat{\mathbf{u}}_{\mathbf{j}}$ are, respectively, perpendicular and parallel to each other.

III Simulation results

A Simulation details

The phase behaviors of systems (i)-(iii) were studied over a range of sphere concentrations using constant NVT molecular dynamics (MD) and constant NPT Monte Carlo (MC) techniques. Simulations of 50/50 mixtures were performed using $N = 1024$ particles in total, whereas twice as many particles were used at lower sphere concentrations, the numbers of rods and spheres being adjusted to provide each desired concentration.

In the MD simulations, the Velocity Verlet algorithm [16] was employed with a time step $\delta t = 0.0015\sqrt{m\sigma_0^2/\epsilon_0}$. At each state point, the system was equilibrated for at least 5×10^5 time steps followed by a production run of 2×10^5 time steps. Observables were calculated every 200 time steps and then averaged. Periodic boundary conditions, minimum image convention, and Verlet neighbor list were applied. The intermolecular potentials were truncated and shifted at a distance $r_c = 4\sigma_0$. The masses of the rods and spheres were set to unity as were the moments of inertia about the short axes of the rods. In the MC simulations, standard random particle

displacement moves were applied and random rotations for the rods were implemented using the Barker-Watts method [17]. N such random MC moves made up one MC cycle, so that, on average, each particle experienced one trial move per cycle. The three simulation box side lengths were allowed to change independently to provide constant pressure conditions in the system. The corresponding particle coordinates were rescaled proportionally to the side length changes, 5 such moves being attempted in each MC cycle.

In the following, all quantities are expressed in reduced units. This means that distance is measured in units of σ_0, energy in units of ϵ_0, and temperature in units of ϵ_0/k_B, where k_B is Boltzmann's constant. As a consequence, $\sqrt{m\sigma_0^2/\epsilon_0}$ is the unit of time, ϵ_0/σ_0^3 is the unit of pressure, and the number density, ρ, is measured in units of σ_0^{-3}.

The orientational order parameter, S, and pressure, P, were monitored throughout the simulations. The orientational order parameter was calculated as the ensemble average of the largest eigenvalue of the Q tensor:

$$Q_{\alpha\beta} = \frac{1}{N}\sum_{i=1}^{N}\frac{1}{2}(3u_{i\alpha}u_{i\beta} - \delta_{\alpha\beta}), \tag{11}$$

where $u_{i\alpha}$ is the α component ($\alpha = x, y, z$) of the vector $\hat{\mathbf{u}}_\mathbf{i}$, and $\delta_{\alpha\beta}$ is the Kronecker delta. The pressure was calculated using the virial expression,

$$P = \rho k_B T - \frac{1}{3V}\sum_{i=1}^{N}\sum_{j<i}^{N}\mathbf{r}_{ij}\cdot\mathbf{F}_{ij}. \tag{12}$$

Rod-rod, rod-sphere and sphere-sphere radial distribution functions were also calculated to assess structural properties.

In this study, we have restricted our simulations to ensembles in which the particle concentrations are fixed. This constraint raises the prospect that simulations performed in biphasic state points may have adopted metastable arrangements rather than undergoing macroscopic phase separation. In lattice model simulations of such systems, the semi-grand canonical ensemble has been shown to offer an effective route to avoiding such difficulties [8]. Here, however, our primary aim has not simply been to locate phase coexistence boundaries; we have also investigated the anchoring properties of the various LC-isotropic interfaces available to this class of

system. This has necessitated the use of ensembles in which direct phase coexistence is supported, but has relied on careful assessment of hysteresis and metastability effects, largely through reproducibility of results, for the setting of phase coexistence boundaries.

Before going on to describe the results obtained in this study, it is informative, at this point, to summarize previous findings for both the pure Gay-Berne parameterization employed here [13] and hard particle rod-sphere mixtures [10]. The pure Gay-Berne fluid is known to exhibit isotropic, nematic, and smectic phases [13, 18], the triple point temperature of isotropic-nematic-smectic coexistence being $T_0 = 0.85$. Hard particle rod-sphere mixtures based on the same shape parameters as those used in the current study undergo an isotropic-nematic transition on compression for sphere concentrations in the range $0\% \leq c < 50\%$ [10]. The volume-fraction of this transition increases approximately linearly with sphere concentration until, for $c \gtrsim 50\%$, compression of the homogeneous isotropic phase leads directly to macrophase separation into rod-rich nematic and sphere-rich isotropic phases.

B System (i)

The first system (i) mixture to be investigated contained 512 spheres and 512 rods, originally equilibrated into a homogeneous isotropic phase at temperature $T = 2T_0 = 1.70$ and number density $\rho = 0.40$. Initially, this configuration was subjected to a cooling sequence of MD runs down to $T = 0.70$. Subsequently, two equilibrated configurations from this sequence, corresponding to high, $T = 1.50$, and low, $T = 0.70$, temperatures, were used as the starting points of isothermal compression sequences of MD runs covering the density range $0.40 \leq \rho \leq 0.50$. Finally, several further runs were undertaken at various concentrations and temperatures in order to clarify certain features of the approximate phase diagram shown in Fig. 2. These simulations, performed at the points marked with diamonds on Fig. 2, were run on from configurations previously equilibrated at neighboring state points. The resulting phase diagram shows isotropic mixed and isotropic demixed regions, as well as extensive areas of nematic-isotropic and smectic-isotropic phase-coexistence.

The dashed line on Fig. 2, which represents the boundary between mixed and

demixed regions, was determined from changes in the sphere-sphere radial distribution function, $g_{ss}(r)$. For example, Fig. 3, which shows $g_{ss}(r)$ calculated at number density $\rho = 0.40$ and temperatures $1.2 \leq T \leq 1.4$, indicates formation of sphere-rich domains in this temperature range. Configuration snapshots taken from the $T = 1.2$ run confirm this, showing a single sphere-rich droplet coexisting with an isotropic rod-rich phase. This demixing line was found to shift to slightly higher temperatures with increase in density and, for the temperature range considered here, always remained distinct from the order-disorder transition of the rod-rich phase. This is consistent with the fact that the analogous mixture of hard particles forms a homogeneous isotropic phase at these densities but phase separates into rod-rich nematic and sphere-rich isotropic phases at $\rho \approx 0.51$ [10].

The compression sequence performed at $T = 1.5$ did not reveal any transitions in the system, but a weak tendency to demix was seen at the higher densities. Table II shows how the energy, order parameter and pressure changed along the $T = 0.7$ isotherm. Here, the increase of the nematic order parameter indicates a phase transition at a density of about $\rho = 0.45$. At densities above this, the rod-rod distribution function measured parallel to the director, $g_{\parallel}(r_{\parallel})$, showed periodic density waves, characteristic of the smectic B phase formed by the pure Gay-Berne fluid at this temperature [18]. The rod-rod and sphere-sphere radial distribution functions calculated for this system at $\rho = 0.42$ and $\rho = 0.47$ are shown in Fig. 4. These indicate that the structure of the sphere-rich phase remained almost unchanged in this density range, implying that the density changes were accommodated by rearrangement of the rod-like particles. The $g_{ss}(r)$ curves also indicate demixed configurations at both of these state points.

According to configurational snapshots (see, e.g., Fig. 5), the spherical particles formed a droplet at all densities for $T = 0.70$. At all but the lowest densities, this droplet was found to be cylindrical, looping around on itself as an artifact of the periodic boundary conditions. The presence of this cylinder of spheres provided this system with an axis of symmetry which was found to have some influence the orientational distribution functions of the rods. Test runs showed, however, that while the topology of the droplet had the expected strong system-size dependence,

the phase behavior shown in Fig.2 was robust to such changes. In the absence of this symmetry-breaking artifact, we would expect the director to lie randomly in the plane of a flat LC-isotropic interface; for this system, the general tendency of rods to align in the plane of a featureless substrate [19] is accentuated by the strong rod-sphere side interaction.

On increasing the temperature of the higher density smectic configurations, the periodic density waves dispersed to leave a rod-rich nematic phase. Location of the boundaries of the nematic region of the phase diagram was made difficult by the interfacial ordering induced by the cylinder of spheres. That said, this system proved relatively free of the pre-transitional order parameter fluctuations that characterize the nematic-isotropic transitions of single component Gay-Berne systems.

Further simulations of system (i) at sphere concentrations of 20% and 10% showed that, at similar packing fractions, the demixing temperature was shifted to lower values than those found for the 50/50 mixture. At a sphere concentration of 20%, for example, the system remained homogeneous at temperatures as low as $T \approx 0.9$ at low densities (see Fig. 6). A qualitative difference between the 50/50 and 80/20 phase diagrams was that in the latter the isotropic-isotropic demixing was superseded by isotropic-nematic phase coexistence when cooling at high densities. This crossover is explained by the fact that the equivalent hard particle system exhibits a homogeneous isotropic-nematic transition at $\rho \approx 0.37$. This trend was followed by the 90/10 rod-sphere mixture of system (i), for which no demixed isotropic phases were found for $1.20 \geq T \geq 0.50$ [20]. Here, only phase separation was observed, that is a droplet of spheres suspended in either a nematic or a smectic rod-rich phase.

C System (ii)

A 50/50 system (ii) mixture was found to demonstrate strong isotropic-isotropic demixing for a similar range of temperatures to that found with system (i). Here, the simulations were initiated at high temperature ($T = 1.5$) and the mixture was compressed from $\rho = 0.40$ up to $\rho = 0.50$. The nematic order parameter measured during this compression sequence indicated that the rod orientational distribution function remained isotropic over the whole range of densities. The sphere-sphere

radial distribution functions suggested, however, that this compression had been performed close to the demixing line, crossing it at $\rho \approx 0.49$. A subsequent cooling sequence, performed with a cubic simulation box at $\rho = 0.42$, revealed that, on demixing, the sphere-rich phase of this system also formed a boundary-condition-stabilized cylindrical droplet. Here, though, the cylinder of spheres was surrounded by rods aligned perpendicular to the its surface (i.e. radially). Due to the orientational defects required by a 2-dimensional periodic array of such structures, this caused significant distortion of the director field, making this series of simulations unsuitable for a detailed analysis of the phase behavior of the rod-rich phase.

To allow study of the phase coexistence in this system in the absence of this topological effect, a second cooling sequence was performed using an elongated simulation box of dimensions $9.261 \times 9.261 \times 25.403$. The intention here was to use the effects of surface tension to promote a pair of planar interfaces parallel to the xy-plane. The initial configuration for this sequence was obtained by applying a non-symmetric constant volume MC move to an initially cubic box at density $\rho = 0.47$ and high temperature ($T = 1.70$). Other than at very low temperatures (see below) subsequent simulations employed constant NVT ensemble MD methods at a fixed box geometry and a range of temperatures: constant pressure and constant volume MC methods both failed when applied to this system because the shortest simulation box side half length became too close to the radius of the Verlet neighbor list, $R_L = 4.5\sigma_0$. At least 10^6 MD time steps were used for equilibration at each temperature. During production runs, any possible demixing was assessed by calculating the density profiles for rods and spheres along the longest simulation box side and averaging over 5×10^5 time steps at each temperature. In compiling these profiles, the z-coordinate of the center of mass of the sphere distribution function was always aligned with the central bin of the analysis histogram.

The resulting concentration distributions, shown in Figs. 7, indicate small non-uniformities at $T = 1.70$ and coexisting sphere-rich and rod-rich regions at lower temperatures. With decreasing temperature, these concentration differences increased in both the rod-rich and sphere-rich regions, even when the former was still in the isotropic phase (Fig. 7(b)). An increase was seen in the nematic order parameter

at a temperature of about $T = 1.20$, indicating an orientational phase transition. This was classified as an isotropic-nematic transition since no layering was seen in the rod-rod distribution function resolved parallel to the director. The sphere-rich phase became totally free of rods at this point, whereas some spheres continued to reside in the rod-rich phase (Fig. 7(c)) at a level of about 9% of that expected for a homogeneous mixture. The nematic director adopted an orientation parallel to the z-axis of the simulation box because the rods close to the two isotropic-nematic interfaces were aligned homeotropically. In order to maintain the isotropy of the pressure tensor on approaching the smectic region [21], a constant pressure MC run was performed at $T = 0.70$ and $P = 2.0$. Under these conditions, the equilibrated simulation box dimensions became $9.36(\pm.05) \times 9.16(\pm.04) \times 24.90(\pm.12)$, corresponding to a density of $\rho \approx 0.48$. As shown by Fig. 7(d), this gave an arrangement comprising well-resolved smectic layers lying parallel to the interfaces. It is interesting to note the difference between the periodic density waves of this smectic phase, and the short-range interfacial features exhibited by the nematic phase in Fig. 7(c).

The properties of system (ii) were also studied at a rod-sphere concentration ratio of 80/20. For this, a system of 1638 rods and 410 spheres was equilibrated at $\rho = 0.30$ and $T = 1.0$ for 1.4×10^6 time steps. Here the sphere-sphere radial distribution function gave high values at short range but approached unity at large separations, suggesting local clustering of the spheres but a random distribution of such clusters. At this state point, 153 ± 17 clusters were found of spheres separated by distances greater than $1.5\sigma_0$. Of these, 7 clusters were relatively large (i.e. contained 20 spheres or more), the largest containing 38 ± 13 spheres. By comparison, the 80/20 mixture of system (i) under the same conditions had 182 ± 11 clusters, the largest of which contained 20 ± 4 spheres, and the equivalent mixture of hard particles at the same density contained 248 ± 12 randomly formed clusters, the largest cluster containing only 10 ± 3 spheres.

This enhanced cluster formation in system (ii) was found to have little effect when the system was cooled or compressed gradually: when treated in this way, the clusters of spheres merged to form a single large droplet suspended in a rod-rich solvent. When, however, the equilibrated $\rho = 0.30$, $T = 1.0$ configuration was

quenched down to $T = 0.70$, complete coalescence of the clusters was no longer achieved. Instead the majority of the spheres went on to form 4 distinct clusters containing an average of 85 spheres each (Fig. 8). Having developed, this arrangement remained relatively unchanged even after an extended run of 3.0×10^6 time steps. The longevity of this metastable multi-droplet configuration can be explained by the well-defined layer of rods which formed around each cluster during the early stages of the quench. Once formed, these layers prevented the droplet surfaces from coming within touching distance of each other, so making coalescence impossible. This effective emulsification of the sphere-rich droplets is noteworthy since it introduces the prospect of observing microphase separated arrangements in rod-sphere systems.

D System (iii)

Before presenting the results for this system, we recall that the strength of the rod-sphere interaction in system (iii) has no orientational dependence and is characterized by a constant well depth ϵ_0. Since this is equal to the strongest well-depths available to the rod-sphere interactions considered in systems (i) and (ii), the average rod-sphere interaction strength for any liquid-like configuration of system (iii) will necessarily be greater than those of the systems considered in the preceding Sections. For this reason, system (iii) can be expected to show a reduced tendency to exhibit demixing and phase separation.

Initially, two compression sequences of MD runs were performed on 1024-particle 50/50 rod-sphere mixtures of system (iii) at relatively high ($T = 1.20$) and relatively low ($T = 0.70$) temperatures over the range of densities $0.40 \leq \rho \leq 0.50$. At both temperatures, these systems remained orientationally isotropic and compositionally homogeneous over the entire density range and no discontinuities were seen in the structural and thermodynamic observables. Superficially, this could be taken to be a reflection of the behavior of the equivalent hard particle system [10], which also behaves in this way prior to phase separating at $\rho \approx 0.51$.

On comparing the rod-rod radial distribution functions, however, the system (iii) configurations were found to contain a significantly higher proportion of rod

side-by-side arrangements than the equivalent hard particle system. Subsequently, two short cooling series were performed, at low, $\rho = 0.42$, and high, $\rho = 0.48$, densities. Starting from configurations previously equilibrated at $T = 0.70$, the system was cooled to $T = 0.60$ and then further to $T = 0.50$. Even at these low temperatures, the nematic order parameter remained low at both densities. However, configuration snapshots indicated the development of local structure: fragments of smectic-like monolayers and sphere-rich sheets were observed. The sphere-sphere radial distribution functions calculated during these cooling sequences (Fig. 9) showed an increase in structural regularities of this type, while cluster analysis indicated development of a bicontinuous interconnected network, i.e. there were no separate clusters of spheres. Since some of the growing features seen in the distribution functions, *e.g.* that at 5-6σ_0 in Fig. 9, were at distances approaching the simulation box side half-length, a series of much larger simulations was employed to study this system more fully. In particular, it was felt necessary to investigate whether the structure observed in these 1024-particle simulations was a non-equilibrium arrangement, frustrated by the relatively high cooling rate and/or the need to be commensurate with the periodic boundary conditions, but metastable with respect to a lamellar phase (i.e. planar layers of rods separated by layers of spheres).

To this end, further simulations were performed on a significantly larger system (iii) mixture subjected to a moderate cooling rate. Here, a system comprising 8192 rods and 8192 spheres was simulated on two 64 node parallel machines (SG Origin 3000 and Cray T3E-1200E) at CSAR in Manchester. The software used to perform these simulations was a version of the domain-decomposition parallel MD code GBMOLDD [22] modified so as to include the specific rod-sphere interaction described in Section II. The initial configuration for these simulations was obtained by replicating eight images of a simulation box of 2048 hard particles, so giving a system of 16384 particles in total. In order to prevent simulation of eight identical configurations in parallel, the initial translational velocities were randomized according to the Maxwell-Boltzmann distribution [16].

A complete list of the large system runs, in the order in which they were performed, is given in Tab. III. Initially, a $\rho = 0.40$ system was cooled from $T = 0.6$ to

$T = 0.55$. Linear extrapolation indicated that further cooling at this density would have caused the pressure to go negative, therefore, the system was then compressed at $T = 0.55$ to $\rho = 0.42$. Following this, a second cooling and compression sequence was performed down to the state point $T = 0.51$, $\rho = 0.45$. Throughout this series of runs, the temperature and density dependence of the potential energy was approximately linear. Thus, no discontinuities were observed in the potential energy or its first derivatives while the system transformed from the uniform isotropic configuration to that shown in Fig. 10. Similarly, no discontinuous changes were observed in any of the measured distribution functions or in the cluster analysis data.

For this system, cluster analysis (based on sphere-sphere separations of 1.5σ or less) showed that, even in the relatively isotropic and uniform configuration at $T = 0.60$ and $\rho = 0.40$, about 95% of the spheres were members of a single continuous network. The extent of this network was found to grow with decreasing temperature and increasing density, such that for $T = 0.51$ it contained virtually every sphere in the system. When combined with the absence of macroscopic phase separation, this indicates that the structure shown in Fig. 10 is a bicontinuous microphase separated network. Figure 11 shows sphere-sphere radial distribution functions measured at the densities considered at $T = 0.51$. In the separation range 0-$6\sigma_0$, they indicate similar behavior to that observed in the equivalent 1024-particle system (c.f. Fig. 9). Furthermore, these functions approach unity at separations greater than $10\sigma_0$, indicating the absence of long-range transitional correlations, and confirming that this system does not develop lamellar order at this concentration ratio.

The temperatures at which microphase separation occurred in this system were relatively low, raising the possibility that the system's state was rather glassy. To check the fluidity of the observed state, the particle mean square displacement was calculated (Fig. 12). In the case of Brownian or random walk motion, the mean square displacement is known to be a linear function of time:

$$< (\mathbf{r}(t) - \mathbf{r}(0))^2 >= 6Dt, \tag{13}$$

where D is the diffusion coefficient. However, this dependence is not linear in the case of some complex systems such as polymers, for example, for which the mean

square displacement is proportional to t^{ν}, where $\nu < 1$ [23]. The double logarithmic scale used in Fig. 12 reveals how the exponent ν changed in the time range 200 $\delta t \leq t \leq 3 \times 10^5 \delta t$. At times up to several thousands time steps, the diffusion of both rods and spheres was not macroscopic due to short time correlations in particle positions. Only after about 30,000 time steps, when each rod (sphere) had moved, on average, $1.3\sigma_0$ ($1.8\sigma_0$) from its initial position did both dependencies became linear. The gradients of the tangents shown in Fig. 12 are almost equal for both curves at $\nu = 0.91 \pm 0.02$. The average rod (sphere) displacement over the total simulation run length at $\rho = 0.45$ and $T = 0.51$ (9×10^5 time steps) was estimated as $5.8\sigma_0$ ($8.3\sigma_0$). These values support the notion that the system was in a fluid state and that the particles were moving in an approximately Brownian manner when in structures such as that shown in Fig. 10.

Finally, in this Section, we report briefly on the behavior of system (iii) mixtures with reduced sphere concentrations. The most interesting structures shown by such systems were found from low temperature compression series of constant NVT runs performed on 70/30 rod-sphere mixtures. For temperatures of $T = 0.6$ and above, such sequences showed that this system underwent macroscopic phase separation at the onset of smectic ordering. However, a compression sequence performed at $T = 0.5$ lead to the formation of a different layered structure, in which the peak-peak separations in $g_{\parallel}(r_{\parallel})$ were significantly larger than those of the usual smectic phase. Cluster analysis performed on these $T = 0.5$ systems (based on sphere-sphere separations of $1.5\sigma_0$ or less) also showed unusual behavior, 10 reasonably large clusters being found for a range of densities. Configuration snapshots confirmed that these observations corresponded to a partially-formed lamellar structure, i.e. layers of rods, approximately half of which sandwiched planes of spheres.

In order to establish the thermodynamic stability of this lamellar arrangement, auxiliary MC runs were performed in the constant NPT ensemble, including the use of non-uniform volume change moves so as to reduce the effects of the periodic boundary conditions. While these simulations proved very slow to stabilize (2×10^6 MC sweeps were required at $P = 1.5$, more than half of which were equilibration), the periodic, microphase separated lamellar structure shown in Fig. 13(a) was found

to persist. The corresponding distribution functions, $g_{ss}(r)$ and $g_{\parallel}(r_{\parallel})$, are shown in Fig. 13(b). Here, the $g_{ss}(r)$ curve shows a broad peak at $r \approx 4.5$, corresponding to spheres separated by layers of rods. Equivalently, the peaks in the $g_{\parallel}(r_{\parallel})$ curves are less well defined than is usual for a Gay-Berne system, showing contributions from both neighboring smectic layers and smectic layers separated by layers of spheres. The relative complexity of this structure explains its slow equilibration; compositional microphase separation throughout the system and commensurability between the layer spacings and the boundary conditions are both required.

On reducing the sphere concentration further, to 20% by number, the behavior of system (iii) at moderate temperatures was found to be very similar to that of the equivalent hard particle system. For instance, compression of such a mixture at $T = 1.0$ lead to formation of a compositionally homogeneous (i.e. well mixed) nematic phase at $\rho \approx 0.38$. At lower temperatures, e.g. $T = 0.7$, equivalent compression sequences resulted in the development of a smectic phase containing small clusters of spheres. Here, however, the sphere clusters appeared as random inclusions, rather than being regularly spaced, and so no lamellar structures were observed.

IV DISCUSSION AND CONCLUSIONS

In this paper, we have focused on the influence of the rod-sphere interaction on the phase behavior of binary mixtures of rod-shaped Gay-Berne particles and small Lennard-Jones spheres. From this, we have found that such mixtures exhibit a rich and fascinating phase behavior which is sensitive to the strength and symmetry of the rod-sphere interaction, as well as the species concentration ratio.

System (i), in which the spheres were most attracted to the sides of the rods, exhibited strong demixing: at sphere concentrations of 10%, 20%, and 50%, the mixture components separated macroscopically before the onset of any orientational order. The anisotropy of the rod-sphere potential was inverted in system (ii), such that the end interaction was made 5 times as strong as the side interaction. This system was found to show stronger demixing than system (i) at 50/50 rod-sphere concentration ratio, and at low sphere concentrations it could be quenched into

metastable multiple-droplet arrangements.

Additionally, the sphere-rich–rod-rich phase boundaries established in these demixing and phase separating systems were found to have well-defined anchoring properties. Tangential anchoring was found in system (i), whereas normal anchoring was seen in system (ii). This raises the prospect of being able to control both the strength and symmetry of anchoring behavior simply through appropriate modification of the rod-sphere interaction anisotropy ϵ_S/ϵ_E. We also note that the structures associated with these fluid-fluid phase boundaries were qualitatively similar to those seen previously at the liquid crystal-vapor interface, rather than the highly stratified arrangements seen for liquid crystals adsorbed at solid substrates [24]. This class of system, therefore, appears a viable route towards the development of a simulation system capable of genuinely accessing the weak anchoring regime.

Phase behavior equivalent to that observed in these systems has also been seen experimentally in, for example, the phase separating oil plus LC mixtures used by Loudet and co-workers in their studies of LC colloid systems [2]. Because of the considerable time- and length-scale differences involved, the processes governing the formation of the highly monodisperse, microscopic oil droplets observed in ref [2] are not fully accessible to the models used here. However, our simulations do appear well suited for the investigation of early stage phase-separation dynamics and the metastability of very small droplets formed in deep quenches (as a function of the molecularly controllable interfacial properties).

In system (iii), by contrast, the use of a stronger average rod-sphere interaction weakened the tendency of the particle types to demix, resulting in the formation of microphase separated structures. Thus, for a 50/50 rod-sphere concentration ratio, the diluting effects of the spherical particles proved sufficient to prevent conventional LC phases from forming. Instead, a bicontinuous network developed, containing highly curved monolayers of rods with smectic-like in-layer order. Similarly, at a sphere concentration of 30%, long-ranged orientational order was only achieved through expulsion of the spheres to the interlayer spacings of a lamellar smectic arrangement.

System (iii) provides an example of the microphase separation that can result

when a mixture containing a significant concentration of mesogenic particles is frustrated from forming an LC phase due to the continued integration of a significant non-mesogenic component. In the system considered here, macrophase separation has been resisted because the rod-sphere interaction was relatively strong; this countered the net entropic drive for such a system to phase separate at high density due to the inefficient packing of the rods and spheres [10]. However, it appears that the system considered here is just one of many in which hybrid structures may arise due to the compromise forced on one component with a strong desire to order by a second which does all it can to resist: from such conflicts, originality often flows. In addition to this compositionally resisted mesophase formation, the Brownian dynamics exhibited by the particles in system (iii)'s microphase separated structures also raises intriguing possibilities; to this end, both the rheology and the field-swithability of these phases will be investigated in future studies.

ACKNOWLEDGEMENTS

We gratefully acknowledge the financial support of the MRI in providing a studentship for D.A., and EPSRC for providing computational hardware under grant GR/L86135. We also wish to thank Prof. C. M. Care for useful conversations, Prof. M. E. Cates giving us access to CPU time on the Manchester CSAR service, under EPSRC grant GR/M56234/01, and Dr. R. Webster for his assistance in the submission and running of these CSAR simulations.

References

[1] T.W. Cheung, S. Fan, G.R. Luckhurst and D.L. Turner, J. Chem. Soc. Faraday Trans. **93**, 3099 (1997).

[2] J. Loudet, P. Barois, and P. Poulin, Nature **407**, 611 (2000).

[3] O. Mondain-Monval and P. Poulin, J. Phys. Cond. Matt. in press (2004).

[4] G.A. Vliegenthart, A. van Blaaderen and H.N.W. Lekerkerker, Faraday Discuss. **112**, 173 (1999).

[5] M. Adams, Z. Dogic, S.L. Keller and S. Fraden, Nature **393**, 349 (1998).

[6] T. Koda, M Numajiri and S. Ikeda, J. Phys. Soc. Japan **65**, 3551 (1996).

[7] Z. Dogic, D. Frenkel, S. Fraden, Phys. Rev. E **62**, 3295 (2000).

[8] R. Hashim, G.R. Luckhurst and S. Romano, Proc. Roy. Soc. Lond. A **429**, 323 (1991); M.A. Bates, Phys. Rev. E **65**, 041706 (2002).

[9] H. Bosetti and A. Perera, Phys. Rev. E **63**, 021206 (2001); M. Schmidt, Phys. Rev. E **63**, 050201(R) (2001).

[10] D. Antypov and D.J. Cleaver, Chem. Phys. Letts. **377**, 311 (2003).

[11] F. Vesely, unpublished (2003).

[12] J.G. Gay and B.J. Berne, J. Chem. Phys. **64**, 3316 (1981).

[13] E. De Miguel, L.F. Rull, M.K. Chalam, and K.E. Gubbins, Molec. Phys. **74**, 405 (1991).

[14] B.J. Berne and P. Pechukas, J. Chem. Phys. **56**, 4213 (1972).

[15] D.J. Cleaver, C.M. Care, M.P. Allen and M.P. Neal, Phys. Rev. E **54**, 559 (1996).

[16] M.P. Allen and D.J. Tildesley, *Computer Simulation of Liquids*, OUP (Oxford, 1986).

[17] J.A. Barker and R.O. Watts, Chem. Phys. Letts. **3** 14 (1969).

[18] E. de Miguel, E. Martín del Río, J.T. Brown and M.P. Allen, J. Chem. Phys. **105**, 4324 (1996).

[19] M. Dijkstra, R. van Roij and R. Evans, Phys. Rev. E **63**, 051703 (2001).

[20] D. Antypov and D.J. Cleaver, J. Phys. Cond. Matt. accepted (2004).

[21] H. Domínguez, E. Velasco and J. Alejandré, Molec. Phys. **100**, 2739 (2002).

[22] J. Ilnitskyi and M.R. Wilson, Comp. Phys. Com. 134, 23 (2001).

[23] M.P. Allen and D.J. Tildesley, *Computer Simulation in Chemical Physics*, Kluwer Academic Publishers (1993).

[24] G.D. Wall and D.J. Cleaver, Molec. Phys. **101**, 1105 (2003).

List of tables

TABLE I. Energy parameters for the rod-sphere potentials of the three systems studied. ϵ_{RS}, ϵ_S, and ϵ_E are given in units of ϵ_0.

System	ϵ_{RS}	ϵ_S/ϵ_E	ϵ_S	ϵ_E
(i)	1	5	1	0.2
(ii)	0.2	0.2	0.2	1
(iii)	1	1	1	1

TABLE II. Potential energy per particle, U_p, the nematic order parameter, S, and pressure calculated on $0.40 \leq \rho \leq 0.50$ at $T = 0.7$ for the 50/50 system (i) mixture. The numbers in brackets represent the statistical uncertainty in the last two digits.

ρ	U_p	S	P
0.40	−3.972(30)	0.074(27)	1.03(08)
0.41	−4.064(31)	0.084(37)	1.17(08)
0.42	−4.145(28)	0.101(44)	1.37(09)
0.43	−4.207(29)	0.142(61)	1.58(08)
0.44	−4.281(33)	0.181(88)	1.82(10)
0.45	−4.402(41)	0.485(49)	1.93(12)
0.46	−4.536(55)	0.658(63)	2.07(10)
0.47	−4.910(33)	0.856(16)	1.85(10)
0.48	−5.050(32)	0.891(11)	2.04(10)
0.49	−5.149(32)	0.912(08)	2.32(11)
0.50	−5.241(32)	0.926(06)	2.67(11)

TABLE III. Simulation details of the CSAR-based runs performed on a 50/50 system (iii) mixture using 16384 particles.

ρ	T	Time steps	U_p
0.40	0.60	350,000	−4.622(8)
0.40	0.58	300,000	−4.691(9)
0.40	0.57	150,000	−4.728(9)
0.40	0.56	300,000	−4.772(8)
0.40	0.55	300,000	−4.812(9)
0.41	0.55	250,000	−4.953(9)
0.42	0.55	580,000	−5.096(9)
0.42	0.54	580,000	−5.147(8)
0.42	0.53	580,000	−5.196(9)
0.42	0.52	500,000	−5.259(8)
0.42	0.51	250,000	−5.315(9)
0.43	0.51	480,000	−5.469(9)
0.44	0.51	440,000	−5.631(9)
0.45	0.51	900,000	−5.799(9)

List of figure captions

FIG 1. Equipotential lines of rod-sphere potentials with different values of the ratio ϵ_S/ϵ_E: (a) $\epsilon_S/\epsilon_E = 5$, (b) $\epsilon_S/\epsilon_E = 1/5$, and (c) $\epsilon_S/\epsilon_E = 1$.

FIG 2. Phase diagram of the 50/50 mixture of type (i). Diamonds indicate state points at which simulations were conducted; dashed line is the demixing line.

FIG 3. Sphere-sphere radial distribution functions of a 1024-particle 50/50 mixture of type (i) at $\rho = 0.40$ and different temperatures.

FIG 4. Sphere-sphere and rod-rod radial distribution functions of a 1024-particle 50/50 mixture of type (i) at $T = 0.70$ before ($\rho = 0.42$) and after ($\rho = 0.47$) the isotropic-smectic transition.

FIG 5. Configuration snapshot of a 1024-particle 50/50 mixture of type (i) at $\rho = 0.45$ and $T = 0.70$.

FIG 6. Phase diagram of the 80/20 rod-sphere mixture of type (i). Diamonds indicate state points at which simulations were conducted; dashed line is the demixing line.

FIG 7. Number density profiles for rods (solid line) and spheres (dashed line) in a non-cubic simulation box along its longest side for a 1024-particle 50/50 mixture of type (ii) at (a) $T = 1.70$, (b) $T = 1.40$, (c) $T = 1.10$, (d) $T = 0.70$. Results (a)-(c) were obtained from the constant NVT MD simulations at $\rho = 0.47$, distribution (d) was calculated from a constant NPT MC run at $P = 2.0$. The dotted lines correspond to the uniform particle distributions.

FIG 8. Configuration snapshot of a 2048-particle 80/20 rod-sphere mixture of type (ii) after a quench at $\rho = 0.30$ from $T = 1.0$ to $T = 0.70$.

FIG 9. Sphere-sphere radial distribution functions, $g_{ss}(r)$, for a 1024-particle 50/50 mixture of type (iii) at $\rho = 0.42$ and a range of temperatures.

FIG 10. Configuration snapshot of a 16384-particle 50/50 mixture of type (iii) at $\rho = 0.45$ and $T = 0.51$. The simulation box side is $33.144\sigma_0$.

FIG 11. Sphere-sphere radial distribution functions, $g_{ss}(r)$, calculated for a 16384-particle 50/50 mixture of type (iii) at $T = 0.51$ and a range of densities.

FIG 12. Time dependence of the mean square displacement of rods (solid line) and spheres (dashed line) calculated for a 16384-particle 50/50 mixture of type (iii) at $\rho = 0.45$ and $T = 0.51$ plotted in the double logarithmic scale.

FIG 13. (a) Configuration snapshot of a 2048-particle 70/30 rod-sphere mixture of type (iii) at $P = 1.5$ and $T = 0.5$ and (b) distribution functions $g_{ss}(r)$ and $g_{\parallel}(r_{\parallel})$ calculated at this data point.

Figure 1. D. Antypov, "Journal of Chemical Physics".

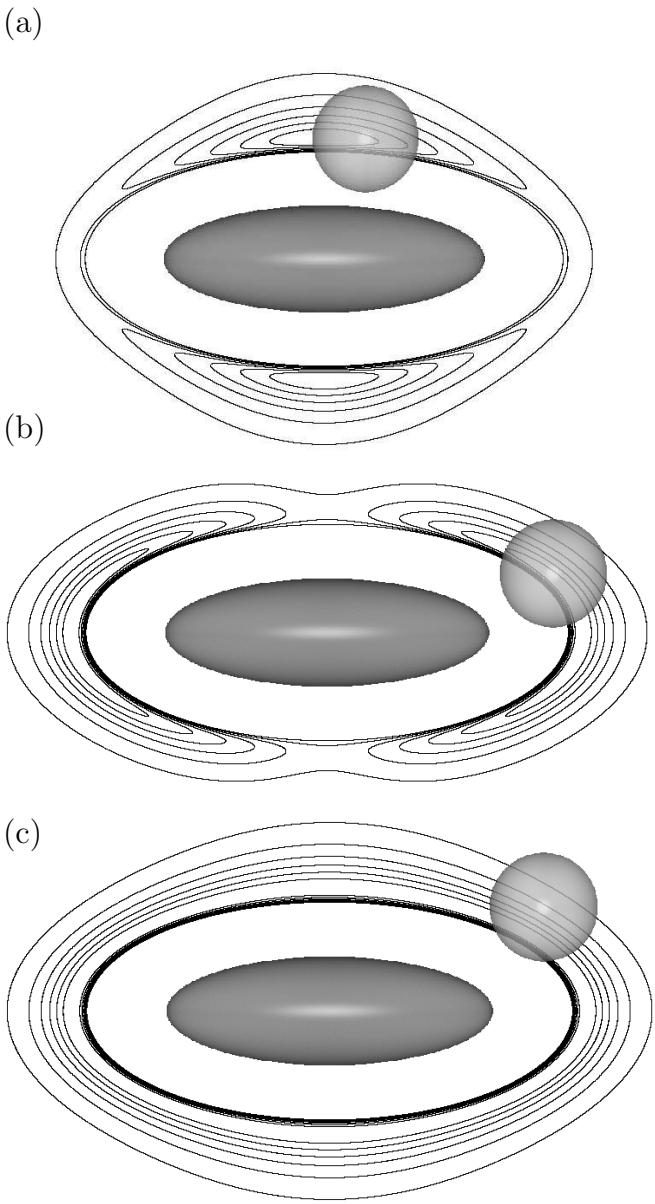

Figure 2. D. Antypov, "Journal of Chemical Physics".

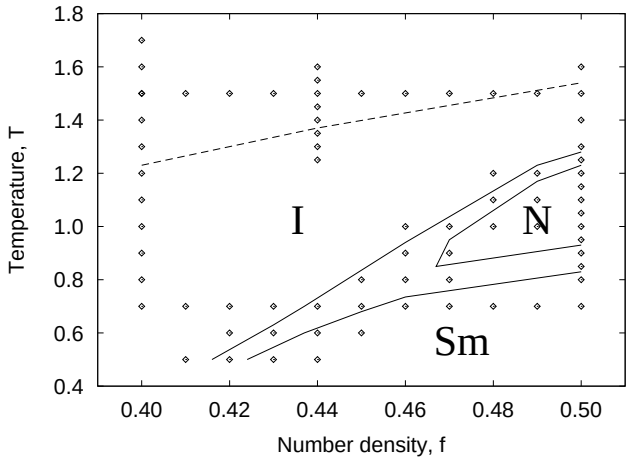

Figure 3. D. Antypov, "Journal of Chemical Physics".

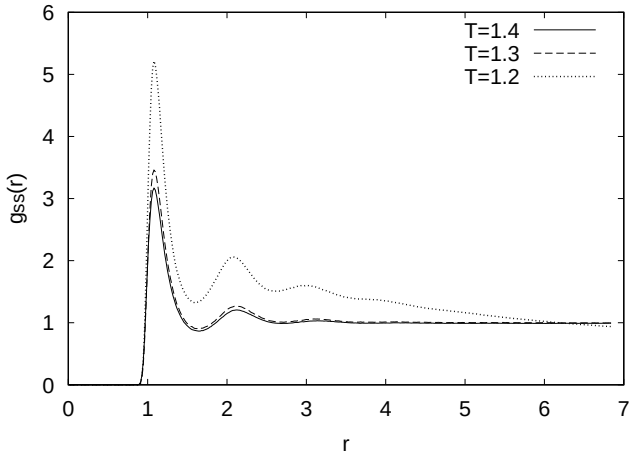

Figure 4. D. Antypov, "Journal of Chemical Physics".

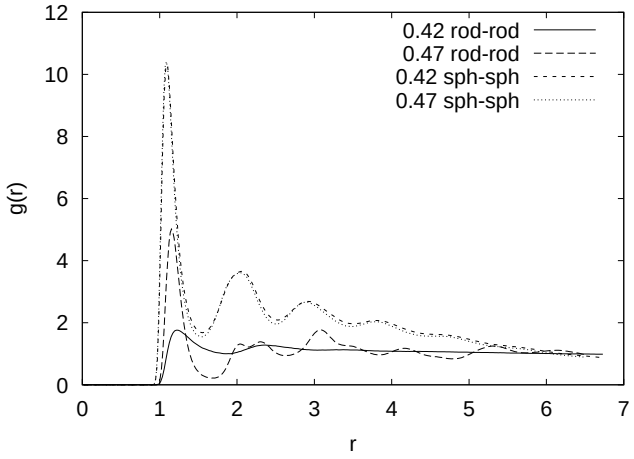

Figure 5. D. Antypov, "Journal of Chemical Physics".

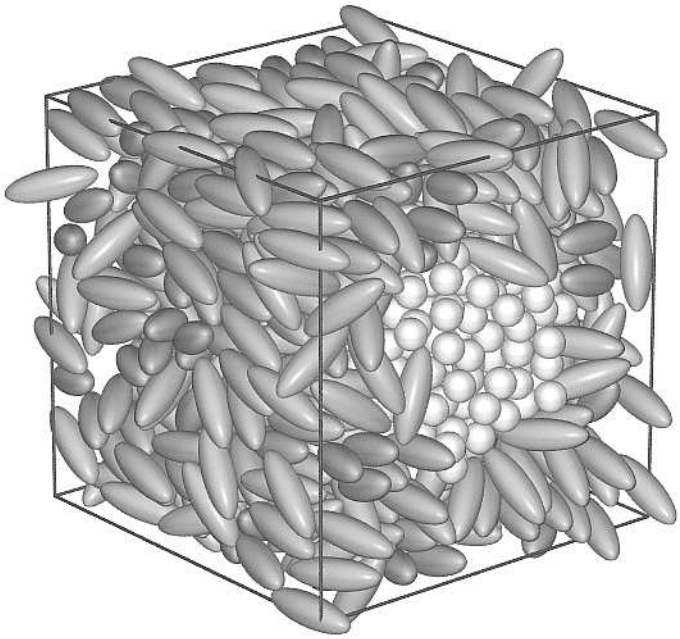

Figure 6. D. Antypov, "Journal of Chemical Physics".

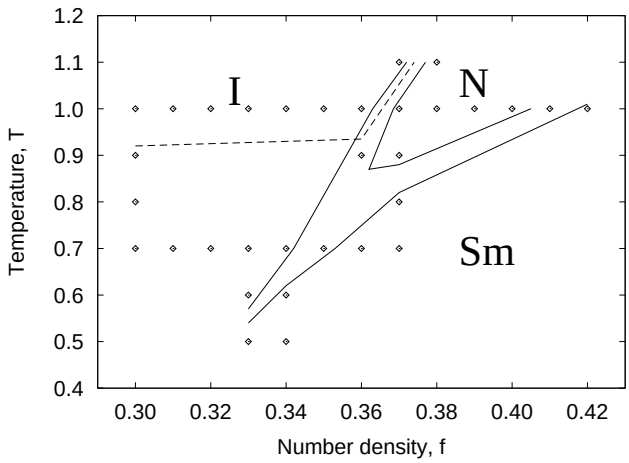

Figure 7. D. Antypov, "Journal of Chemical Physics".

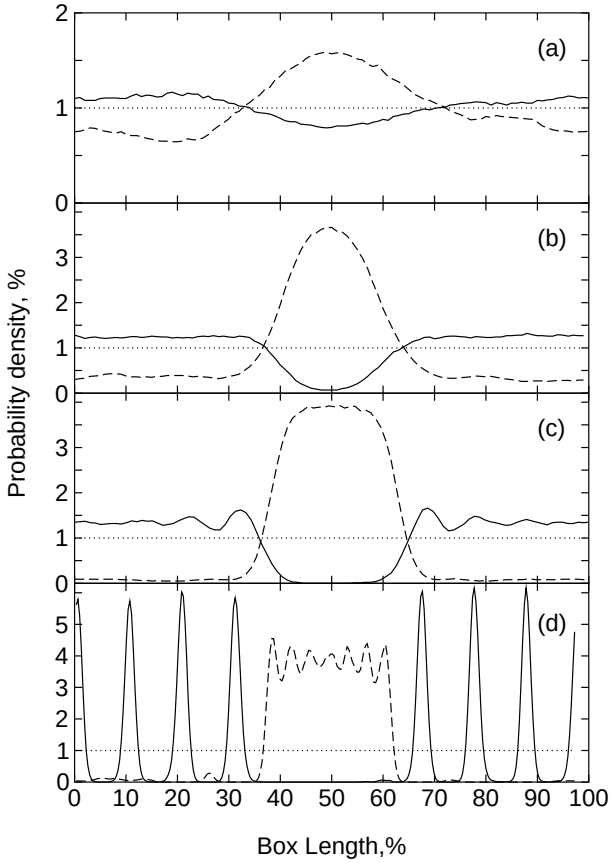

Figure 8. D. Antypov, "Journal of Chemical Physics".

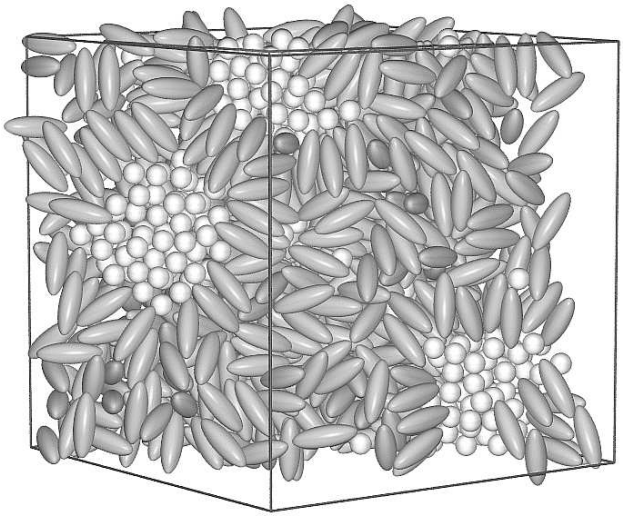

Figure 9. D. Antypov, "Journal of Chemical Physics".

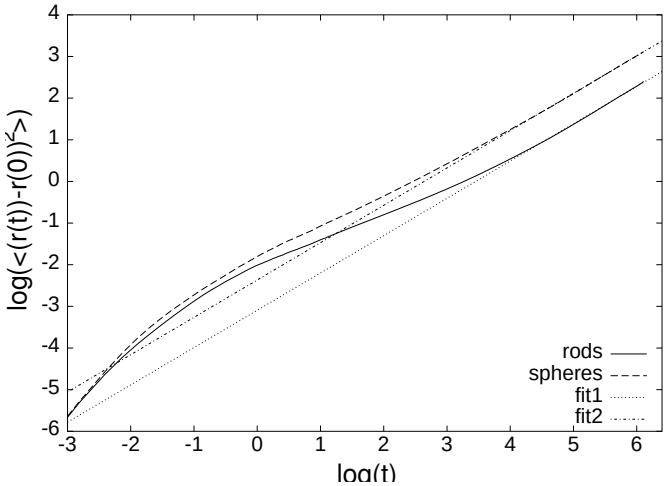

Figure 10. D. Antypov, "Journal of Chemical Physics".

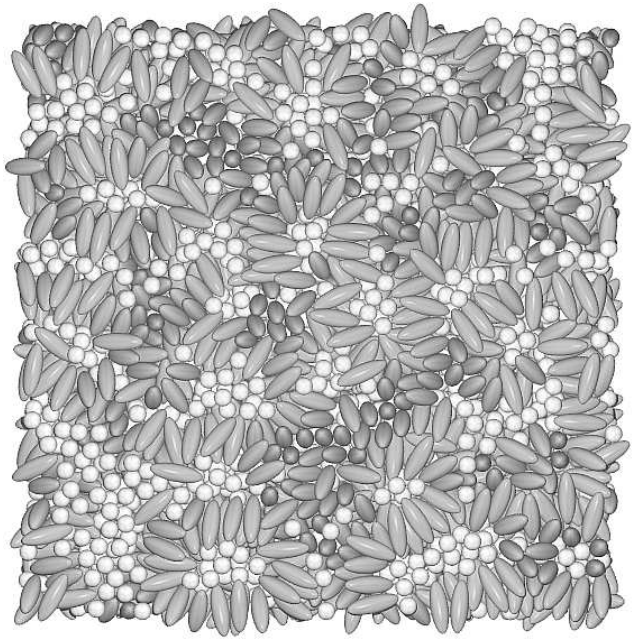

Figure 11. D. Antypov, "Journal of Chemical Physics".

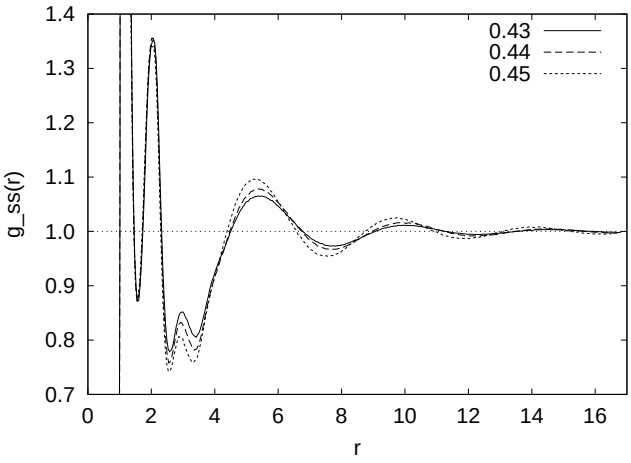

Figure 12. D. Antypov, "Journal of Chemical Physics".

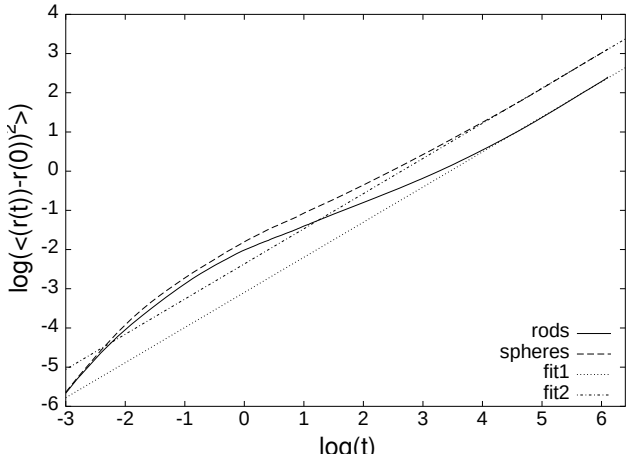

Figure 13(a). D. Antypov, "Journal of Chemical Physics".

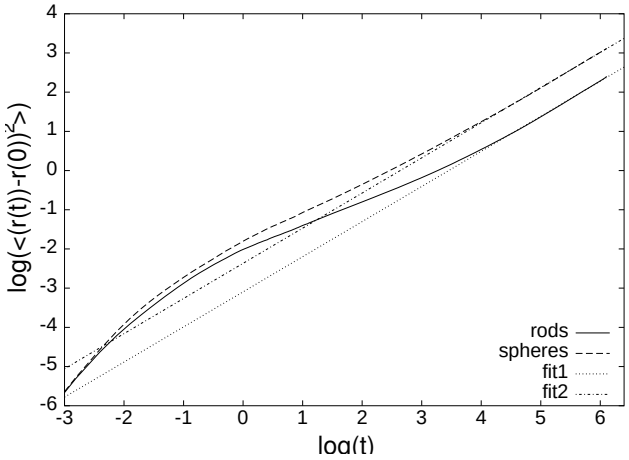

Figure 13(b). D. Antypov, "Journal of Chemical Physics".